Evidence of direct optical transitions in γ-In$_2$Se$_3$

L. de Brucker, M. Moret, B. Gil ⊙, and W. Desrat ⊙*

Laboratoire Charles Coulomb (L2C), Université de Montpellier, CNRS, Montpellier, FR-34095, France

We present an optical study of high crystalline quality γ-In$_2$Se$_3$ films grown epitaxially on (0001)-oriented sapphire. Well-defined structures are detected at 2.147, 2.240, 2.359, and 2.508 eV in the optical absorption at $T = 10$ K. On the basis of the selection rules, we associate them to direct optical transitions with excitons built from the upper and spin-orbit splitoff valence bands and the first conduction band at the Γ point. The first two lowest excitonic peaks vanish from the absorption spectrum above $T = 120$ K at a critical temperature for which the photoluminescence emission fades out as well. It leads us to an estimate of the exciton binding energy of the order of 10 meV in γ-In$_2$Se$_3$. Last, we interpret additional absorption peaks to LO-phonon replicas of the free exciton with a phonon energy of $\sim$14 meV.

I. INTRODUCTION

The van der Wals (vdW) materials are about to revolutionize the optoelectronic components due to their two-dimensional (2D) nature that offers a complete freedom to model tailor-made ultrathin heterolayer-based devices. Their outstanding intrinsic properties promise significant advances in semiconductor applications based on valleytronics, twistronics, or straintronics [1–3]. More specifically, the physics of the ferroelectricity is boosted in vdW-layered compounds with unprecedented mechanisms like the polar stabilization or the switching kinetics, which are reviewed exhaustively in Ref. [4]. One of the spearheads of these materials is α-In$_2$Se$_3$ which reveals nonzero in-plane (IP) and out-of-plane (OOP) polarizations at room temperature as well as a coupling between both components, known as the dipole locking effect, where the switching of one dipole reverses the second one [5–7]. The recent discovery of these unusual properties, i.e., the stability and switchability of the polarization at room temperature, has generated vast research on the 2H and 3R polymorphs of α-In$_2$Se$_3$ [8] from which the ferroelectricity arises due to the noncentrosymmetric crystalline structure of the vdW-stacked layers. A recent study reports that γ-In$_2$Se$_3$ films, which do not have a 2D structure, also exhibit IP and OOP at $T = 300$ K [9]. Therefore research devoted to the enhancement of the crystalline quality of In$_2$Se$_3$ thin films has to be pursued for a finer determination of the polarization properties of the different polytypes of In$_2$Se$_3$. Additionally most of the ferroelectric field-effect transistors are currently fabricated manually from the exfoliation of bulk samples [10,11]. As a consequence the epitaxy of In$_2$Se$_3$ must be developed since good knowledge of the growth will also enable the large-scale production of more complex devices such as multiferroic tunnel junctions [12] and will allow the synthesis of In$_2$Se$_3$-based heterojunctions [13,14]

in which OOP polarization will play a predominant role at the interface.

Historically the γ polymorph has attracted attention among the other polytypes of In$_2$Se$_3$ due to its higher band gap of the order of 2 eV at room temperature which makes it fairly suitable for photovoltaic applications [15]. It has been used as a buffer layer in Mo/CuInSe/In$_2$Se$_3$/ZnO solar cells [16] or as a first growth step in a CuInSe absorber before copper diffusion [17]. This material is potentially interesting for indoor photovoltaics as well, which focuse on the light wavelengths in the visible rather than on the broadband infrared contribution of the solar light spectrum. Like many vdW compounds, the band gap of γ-In$_2$Se$_3$ depends on the number of stacked layers and increases up to 2.5 eV when the film thickness slims down to the monolayer [18].

Bulk crystals of γ-In$_2$Se$_3$ have first been grown by chemical vapor transport in sealed ampoules [18–21]. Single-source and double-source metal organic chemical vapor deposition processes have also been extensively studied to produce thin films [22–24]. The main precursors are H$_2$Se for the chalcogen source and dimethyl- or trimethylindium for the element III [25]. Here we focus on the coevaporation of γ-In$_2$Se$_3$ films from indium and selenium sources [15,26,27]. We report the growth of good crystalline quality γ-In$_2$Se$_3$ epitaxial films on (0001)-oriented sapphire wafers, which exhibit remarkable optical absorption spectra.

II. EPITAXY OF γ-In$_2$Se$_3$ FILMS

The γ-In$_2$Se$_3$ films have been epitaxially grown by coevaporation on (0001)-oriented sapphire substrates in ultrahigh vacuum. The temperature of the indium effusion cell is set at $T_{In} = 790\,^{\circ}$C, which leads to an average growth rate of 500 nm/h. The temperature of the selenium source T_{Se} is tuned in such a way that the ratio of the beam equivalent partial pressures of the VI/III elements is optimized to target the In$_2$Se$_3$ stoichiometry as checked by energy dispersive x-ray spectroscopy. Our optimum growth parameters are $T_{Se} = 195 - 197\,^{\circ}$C and a temperature substrate equal to
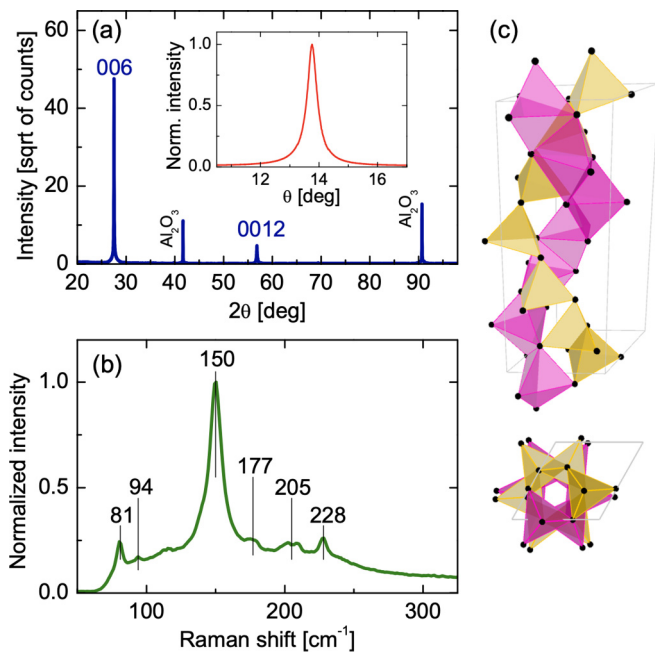
---

*Corresponding author: wilfried.desrat@umontpellier.fr

FIG. 1. (a) $\theta - 2\theta$ x-ray diffractogram of a γ-In$_2$Se$_3$ film grown on (0001)-oriented sapphire substrate. The unit of the XRD intensity is the square root of counts per second. The rocking curve of the main (006) peak is plotted in the inset. (b) The room-temperature Raman spectrum of a γ-In$_2$Se$_3$ film. The thin vertical lines indicate the energies of the vibrational modes. (c) The helical structure of the crystal cell in side and in top views. The black dots represent the selenium atoms.

$T_s = 450\,^\circ$C. It is consistent with the previous studies, which have demonstrated that a sufficient provision of selenium is required for the growth of the selenium-rich phase In$_2$Se$_3$ [15,26–28]. Depending on the growth setups, the formation of this phase occurs for values of the Se/In beams ratio R ranging from 2, similar to our conditions, up to 10. Recently the synthesis of the β polymorph of In$_2$Se$_3$ was reported by molecular beam epitaxy (MBE) for higher T_s and higher values of R [29].

Figure 1(a) shows the $\theta - 2\theta$ x-ray diffractogram of a γ-In$_2$Se$_3$ film, which highlights the preferential orientation of the (00l) planes of the crystallites along the (0001) direction of the sapphire substrate. The detection of the main (006) and (00 12) peaks at 27.532° and 56.837°, respectively, leads to a c lattice parameter of the hexagonal cell equal to 19.42 Å. This is slightly larger than the usual value of 19.38 Å reported for the bulk by only 0.2 % [21,30]. However, it was demonstrated in Ref. [27] that the c parameter could be dependent on the growth temperature of the soda lime glass substrates spanning from 19.38 Å up to 19.44 Å. The formation of grains of a metastable phase competing with the γ phase which induces constraints along the c axis during the growth was suggested for interpreting this observation. Besides, the in-plane lattice parameter a was measured constant in an identical way to what we observe with a value of $a = 7.12$ Å, in perfect agreement with the bulk value [19,21]. The crystallite size along the growth direction is estimated of the order of 150 nm from a simple Debye-Scherrer analysis of the main diffraction peak.

The growth of γ-In$_2$Se$_3$ on crystalline sapphire wafers favors the orientation of the layers and reduces the mosaicity in contrast to the observation reported in the case of the deposition on amorphous glass substrates. The inset of Fig. 1(a) displays the rocking curve of the (006) main peak, whose full width at half maximum is of the order of 0.4°. It remains significant and results from the misorientations of the crystallites out of the c axis of sapphire. It is comparable to the value of 0.55° recently reported for γ-In$_2$Se$_3$ films deposited by MBE on mica [31]. Thus our epitaxial γ-In$_2$Se$_3$ layers grown by coevaporation are of good crystalline quality, which will be confirmed by the optical results presented below. The γ phase unlike the other polymorphs of In$_2$Se$_3$ (α, β, . . .) is not a 2D-layered material and therefore follows more stringent conditions in terms of lattice matching with the substrate than for vdW epitaxy. Thus the nature of the substrate material is likely the main origin of the present crystallographic quality limitations of our In$_2$Se$_3$ films. It is worth noting that the existence of a turbostraticlike stacking which occurs sometimes in 2D compounds, such as boron nitride or graphite [32,33], is ruled out to explain the larger c lattice parameter in our epilayers. The absence of distinct atomic sheets is visible from the 3D crystallographic structure sketched in Fig. 1(c) based on a distorted wurtzite lattice. It is formed by two intertwined screws made of a chain of tetrahedra connected by a common corner and a chain of bipyramids (octahedra) linked by an edge [21]. Selenium and indium atoms are, respectively, at the corners and in the centers of these polyhedra. Interestingly, from this helical shape, it results in a large optical rotary power in γ-In$_2$Se$_3$ [28].

The crystalline quality of our films is further demonstrated by Raman spectroscopy. Figure 1(c) shows the typical Raman spectrum of a γ-In$_2$Se$_3$ sample measured in backscattering configuration at room temperature with a laser wavelength of 473 nm. The high-frequency modes at 81, 94, 150, 177, 205, and 228 cm^{-1} are the clear signatures of the γ polymorph with the prominent peak at 150 cm^{-1} [34,35]. In addition, these experimental values are compared with the computed energies of the vibrational modes [36] listed in the Supplemental Material [37].

III. EXCITONS AND PHONON-ASSISTED ABSORPTION PROCESSES AT LOW ENERGIES

Figure 2(a) presents the main result of this paper, namely, the low-temperature optical absorption of a representative γ-In$_2$Se$_3$ film. The data are reproducible. It has been recorded on four different samples grown with slightly different conditions. A first sharp peak is detected at 2.147 eV close to the absorption edge, followed by successive steps at higher energies (2.240, 2.359, and 2.508 eV) indicated by vertical arrows. An additional plateau at 2.700 eV has to be confirmed. The interaction of the high-energy excitons with the lowest continuum of states broadens them. We suggest that these features are due to direct photon absorption at Γ (i.e., at the center of the Brillouin zone) from the top and the lower spin-orbit splitoff valence bands (VBs) to the first conduction band (CB), as represented in Fig. 2(b) [38].

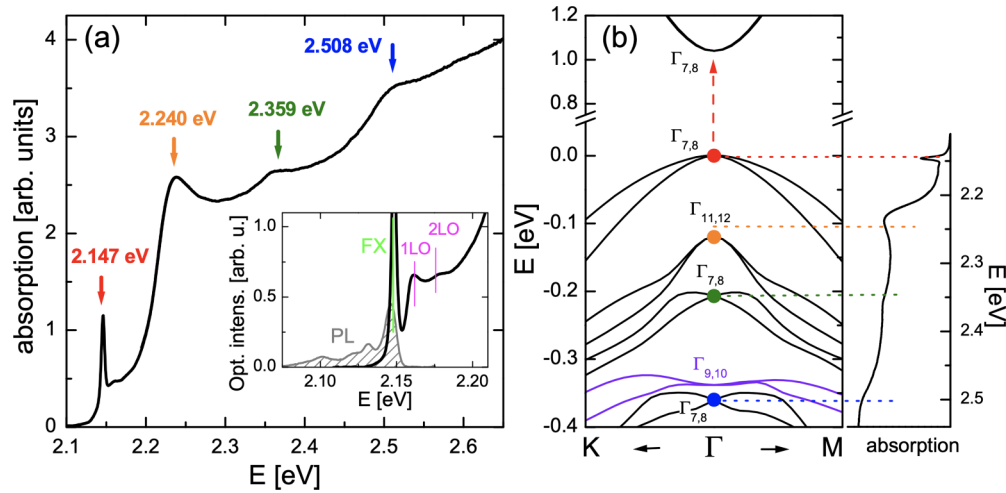First we focus on the close vicinity of the band gap where the absorption curve reveals three peaks at $T = 10$ K [see

FIG. 2. (a) Optical absorption of a γ-In$_2$Se$_3$ film at $T = 10$ K. The arrows highlight distinct features in the absorption curve. The inset focuses on the band-edge region with PL (gray) and absorption spectra (black). (b) Band diagram of γ-In$_2$Se$_3$ around the Γ point along the $K - \Gamma - M$ path in the Brillouin zone. The vertical arrow represents an allowed direct optical transition from the upper VB to the lowest CB at $k = 0$. The colors of the dots and the horizontal lines match with the colors of the arrows in Fig. 1(a).

inset of Fig. 2(a)]. The main peak at $E = 2.147$ eV is undoubtedly the signature of the free exciton (FX), i.e., the $n = 1$ exciton. It was reported previously for polycrystalline γ-In$_2$Se$_3$ but the experimental data were not shown [28]. The second peak at 2.161 eV, 14 meV above, may be attributed to the $n = 2$ exciton. The third peak at 2.177 eV is much broader and looks like the "hump" reported in several semiconductors, such as InSe [39,40]. In the present case, it is obvious that the latter cannot correspond to the $n = 3$ exciton. Indeed from the energies of the $n = 1$ and supposed $n = 2$ peaks one would obtain an exciton binding energy of 19 meV and a $1s - 3s$ splitting of 16.9 meV. The band gap should, therefore, be located at 2.166 eV, that is, below the energy of the hump. Also the 2.161 eV line presents an excessive broadening compared with the width of the 2.147 eV peak. Nothing pleads for this observation in the theory of the dielectric function [41]. Among different origins (3D Sommerfeld factor, interband matrix element, etc.), the most plausible explanation of the side peak is a longitudinal optical (LO) phonon replica of the $n = 1$ excitonic peak in a similar way to what occurs in II-VI materials [42], other monochalcogenides [43], and wurtzitic nitrides [44,45]. In a 1-LO phonon process the phonon energy would be equal to 30 meV. If a 2-LO phonon process is assumed, the second peak, first attributed to the $n = 2$ exciton and located at half energy (i.e. $\sim$14 meV), could be associated to the 1-LO phonon replica. The optical reflectivity data displayed in the Supplemental Material support this identification [37]. The reexamination and our proposal of this peak are supported by the questionable large value of the Rydberg, since the FX peak disappears completely in the optical absorption spectra above $T = 120$ K [Fig. 3(a)]. The photoluminescence (PL) emission vanishes at the same temperature as well [Fig. 3(b)] and, therefore, suggests an exciton binding energy of the order of 10 meV. Hence the interpretation of the 2.161 and 2.177 eV peaks in terms of the 1-LO and 2-LO replica of the $n = 1$ excitonic peak makes sense. The polar phonon of 120 cm^{-1}, i.e., 15 meV, present in the list of the vibrational modes in the Supplemental

Material [37] can account for this energy difference. The second phonon-assisted feature is smoother and broader than the first one, which is also coherent with our interpretation.
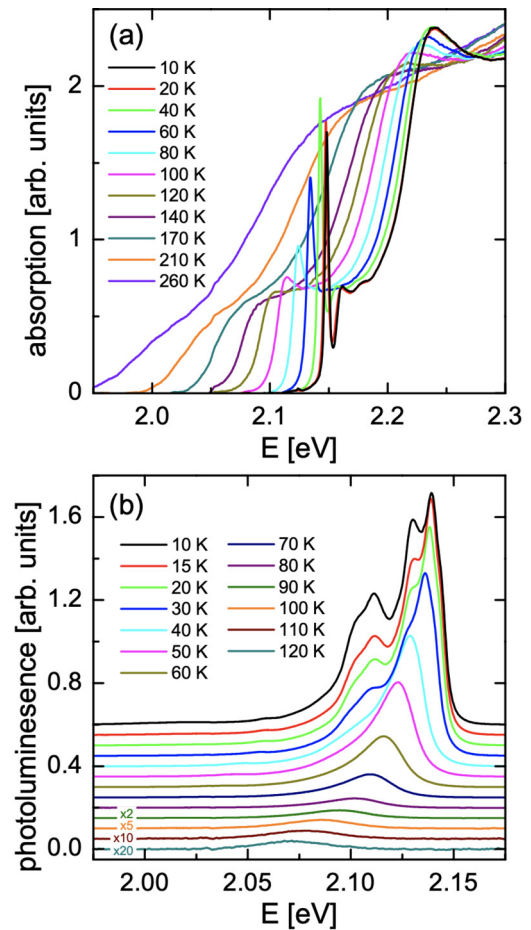

FIG. 3. Temperature dependence of the absorption (a) and PL (b) spectra of γ-In$_2$Se$_3$.
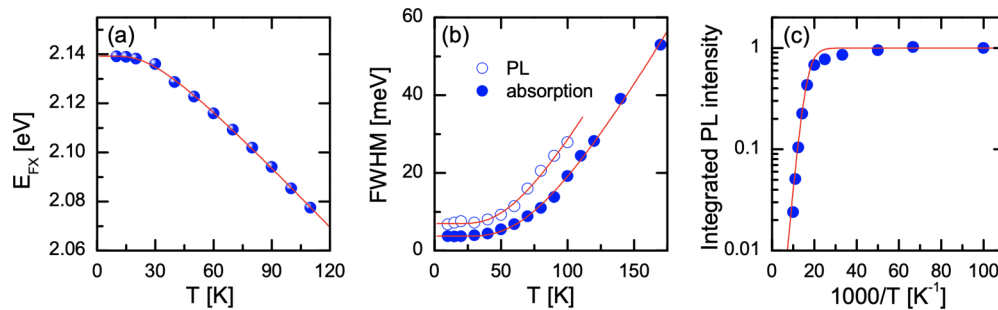
FIG. 4. (a) Energy of the free exciton (FX) peak detected in the absorption vs temperature. (b) FWHM of the FX peak vs temperature measured from the absorption (dots) and the PL spectra (open circles). (c) Arrhenius plot of the integrated whole PL spectrum vs $1000/T$. The solid line is the fit by the single recombination process discussed in the text.

From the temperature dependence of the energy of the FX peak, which is plotted in Fig. 4(a), we can assert that the zero-temperature band gap of γ-In$_2$Se$_3$ equals $E_g(0) \approx$ 2.15 eV in this sample, in agreement with the value reported in Refs. [28,46]. The gap value comes up to 2.16 eV in other samples (see Supplemental Material [37] and the zero-point gap renormalization analysis [47–51]). The dependence of the full width at half maximum (FWHM) of the $n = 1$ peak is traced as a function of T in Fig. 4(b). The fit by the exciton broadening function $\Gamma(T) = \Gamma(0) + \beta/[\exp(\hbar\omega_{ph}/k_BT) - 1]$ leads to a zero broadening $\Gamma(0) = 3.7$ meV for the FX absorption peak, an electron-optical phonon coupling constant $\beta = 157$ meV, and an average phonon energy of 21 meV. The latter is found equal to 17 meV from the PL data. The acoustic phonon contribution proportional to T remains negligible.

The PL was measured as a function of temperature with a Q-switched green laser of 532 nm. The low-temperature traces in Fig. 3(b) show a response composed of several peaks as described earlier [52]. The high-energy peak is the free exciton since its energy corresponds to the one of the $n = 1$ absorption peak Stokes-shifted of about 1 meV at the lowest excitation power [see inset in Fig. 2(a)]. The adjacent peaks were attributed to bound excitons in the past, but phonon replicas could be now considered, as the separation between the two highest peaks is ~14 meV. The PL signal is completely quenched above $T \approx 120$ K whatever the laser power, which was previously reported in Refs. [24,53]. At the opposite, some authors observed the persistence of the PL signal up to room temperature [54,55]. It reveals the predominance of the excitonic emission, without the noticeable detection of deep defects at low T, and of the nonradiative emission at high temperature. The Arrhenius plot of the integrated PL peak intensity is plotted vs $1000/T$ in Fig. 4(c). The data are fitted by a single-channel recombination process,

$$I(T) = \frac{I_0}{1 + AT^{\frac{3}{2}}\exp(-E_a/k_BT)},\tag{1}$$

where the $T^{3/2}$ dependence accounts for the effective density of the band continuum states [56]. The activation energy $E_a \approx 30$ meV is in good agreement with the previous reported values between 25 and 41 meV [17,24,54].

IV. BAND SYMMETRY AND OPTICAL SELECTION RULES

The low-temperature absorption curve presents several steps in the band-to-band region far from the band gap [Fig. 2(a)]. A second absorption edge is detected at 2.240 eV, with a fairly broad excitonic peak that fades out with increasing temperature [Fig. 3(a)]. This situation can be compared qualitatively with what happens in InSe with optical transitions from the p_z-like topmost and lower p_x, p_y-like spin-orbit splitoff VBs to the lowest s-like CB [39,57,58]. In the present case, additional steps at 2.359 and 2.508 eV are detected. We attribute all of these features to direct transitions at $k = 0$ from the upper and subjacent VBs to the lowest CB. The computed band dispersion is shown in the vicinity of the Γ point in Fig. 2(b) (computational details are given in the Supplemental Material [37]). The value of the band gap (~1.05 eV) is far from the experimental value which is inherent to the band computation within the generalized gradient approximation. However, the second CB is located approximately 600 meV above the first CB (see Fig. 2 in the Supplemental Material [37]), while the splittings between the successive VBs are smaller and equal 122, 87, and 132 meV from top to bottom VBs. They are in agreement with the 93, 119, and 149 meV splittings measured experimentally between each kink in the absorption curve. Here we consider that the incorrect underestimated band gap does not alter significantly the dispersion and the energies of the VBs at Γ, which supposes a rigid shift of the bands. Of course a better match could certainly be obtained between the experimental and the theoretical values after an optimized calculation of the bands' dispersion. Taking the spin-orbit coupling into consideration allowed a rather good agreement with the observed VB splittings.

Now we examine the symmetry of the bands to check if the selection rules allow the suggested optical transitions.

The minimum of the CB at Γ transforms like $\Gamma_7 + \Gamma_8$ according to the notations used in Refs. [59,60] that we adopt here. Regarding the VB at Γ, the first five successive states transform like $\Gamma_7 + \Gamma_8$, $\Gamma_{11} + \Gamma_{12}$, $\Gamma_7 + \Gamma_8$, $\Gamma_9 + \Gamma_{10}$, and $\Gamma_7 + \Gamma_8$ in terms of increasing hole energies. The notations $\Gamma_i + \Gamma_j$ are abbreviated as $\Gamma_{i,j}$ in Fig. 2(b). The tables indicate that the symmetry Γ_{dip} of the dipolar operator, which transforms like a polar vector of components $\{x, y, z\}$, is given by different symmetries depending on the orientation of the electric field of the emitted photon: $\Gamma_1(z) + \Gamma_5(x) + \Gamma_6(y)$.

Let Γ_c and Γ_v represent the representations of the conduction and VBs, and let Γ_{env} denote the symmetry of the set of the excitonic envelope functions. The symmetry of the excitonic states is obtained, in the most general case, as the reducible product [61]:

$$\Gamma_c \otimes \Gamma_v^* \otimes \Gamma_{env} = \sum_i \Gamma_{exc}^{(i)}. \qquad (2)$$

In the theory of the hydrogenic atoms, *only* states $\{|n, 0, 0\rangle\}$ of the n kind have the possibility to couple radiatively with the electromagnetic field, which in the language we use here, writes

$$\Gamma_{env} \equiv \Gamma_1. \qquad (3)$$

This equation still holds in our case although, from the cylindrical symmetry around the c axis, these are now the $\{|n, l, 0\rangle\}$ states, with l even, that have the possibility to couple radiatively with the electromagnetic field [62]. In the absence of exciton, the ground state of the crystal is also of Γ_1 symmetry. Therefore the selection rules are at the end obtained by the simple equation

$$\Gamma_c \otimes \Gamma_v^* \otimes \Gamma_{dip} \supset \Gamma_1. \qquad (4)$$

There are two main cases to consider:

(1) When the polarization of the emitted photon is along the z direction, which is equivalent to $\Gamma_{dip} = \Gamma_1$, the selection rules indicate that dipolar excitonic recombinations are allowed for the specific situation when the symmetries of the conduction and VBs are switched from Γ_7 to Γ_8 and vice versa.

(2) When the polarization of the exciton is polarized in the plane orthogonal to z, two (equivalent) cases can be distinguished:

(a) When the electric field of the emitted photon is along the x direction, which is equivalent to $\Gamma_{dip} = \Gamma_5$, dipolar excitonic recombinations are allowed for the specific situation where the symmetries of the conduction and VBs are Γ_7 (resp. Γ_8) and Γ_7 (resp. Γ_{12}).

(b) When the electric field of the emitted photon is along the y direction, which is equivalent to $\Gamma_{dip} = \Gamma_6$, dipolar excitonic recombinations are allowed for the specific situation where the symmetries of the conduction and VBs are Γ_8 (resp. Γ_7) and Γ_8 (resp. Γ_{11}).

This quite abstract description can be simplified if working in the context of an angular momentum representation in a spherical space and using the familiar notations of the textbooks of atomic physics in the context of quantum mechanics. Let as usual J_1 be the spatial angular momentum of the electron wave function and $S = 1/2$ the spin angular momentum. The total angular momentum of the electron scales from $J = J_1 + 1/2$ to $J = J_1 - 1/2$ and given a J, the series of

states $|J, mj\rangle$ is $2J + 1$ times degenerated. The representation D_j that describes the symmetry of the quantum state represented by J is either irreducible or expanded along a series of irreducible representations. According to the tables of Koster *et al.* [59], in the case of the C_6 point symmetry,

(1) Twofold states $D_{1/2}$ $\{|1/2, \pm 1/2\rangle\}$, built from $J_1 = 0$ and $S = 1/2$, transform like $\Gamma_7 + \Gamma_8$;

(2) Fourfold states $D_{3/2}$ $\{|3/2, \pm 3/2\rangle\}$, built from $J_1 = 1$ and $S = 1/2$, transform like $\Gamma_7 + \Gamma_8$ $\{|3/2, \pm 1/2\rangle\}$ and $\Gamma_{11} + \Gamma_{12}$ $\{|3/2, \pm 3/2\rangle\}$;

(3) Twofold states $D_{1/2}$ $\{|1/2, \pm 1/2\rangle\}$, built from $J_1 = 1$ and $S = 1/2$, transform like $\Gamma_7 + \Gamma_8$;

(4) Sixfold states $D_{5/2}$ $\{|5/2, \pm 5/2\rangle\}$, built from $J_1 = 2$ and $S = 1/2$, transform like $(\Gamma_7 + \Gamma_8)\{|5/2, \pm 1/2\rangle\} + (\Gamma_{11} + \Gamma_{12})\{|5/2, \pm 3/2\rangle\} + (\Gamma_9 + \Gamma_{10})\{|5/2, \pm 5/2\rangle\}$).

Obviously the analysis of the selection rules using the representation of the symmetries of the different quantities in terms of the irreducible representations Γ_is is identical to the prescription of the selection rules for optical transitions in the context of the dipolar approximation in atomic physics: $\Delta_j = \pm 1$; $\Delta_{m_j} = 0, \pm 1$ [63]. This teaches us why transitions from $\{|5/2, \pm 5/2\rangle$ to $\{|1/2, \pm 1/2\rangle$ are forbidden. This is indicated by a distinctive color of the corresponding VBs in Fig. 2(b). The symmetry of the second CB (not visible in Fig. 2(b) but in Fig. S2) is $\Gamma_9 + \Gamma_{10}$ and, therefore, all transitions from the VBs to this CB are also forbidden except from the $\Gamma_9 + \Gamma_{10}$ VB in the z polarization and from the $\Gamma_{11} + \Gamma_{12}$ VB for polarizations orthogonal to z. We disregard this possibility as in the energy range of our experiment we should detect only one line and we measured four.

It is interesting to emphasize the identical symmetry for quantum states of the kind $\{|J, \pm \alpha\rangle\}$ for all J of a series discriminatively inside the world of either fermions or bosons, whatever α. This is not a specific quantum effect. It rather comes from the cylindrical symmetry around the z axis and it is a general property encountered for quadratic, trigonal, and hexagonal symmetries [64].

V. CONCLUSION

We demonstrate the epitaxy of high crystalline quality γ-In$_2$Se$_3$ films on (0001)-oriented sapphire substrates, which reveal fine features in the optical absorption at low temperature. Clear excitonic absorption and PL emission processes are demonstrated, which fade out above 120 K in agreement with a Rydberg energy of the order of 10 meV. Three optical signatures are detected at higher energy for the first time, which are associated to direct transitions from the spin-orbit splitoff VBs to the lowest CB which respect the selection rules of the C_6 point group. Thus on top of its ferroelectric properties the γ polytype of In$_2$Se$_3$ has interesting optical properties, which should motivate further experimental and theoretical research.

[1] S. A. Vitale, D. Nezich, J. O. Varghese, P. Kim, N. Gedik, P. Jarillo-Herrero, D. Xiao, and M. Rothschild, Valleytronics: Opportunities, challenges, and paths forward, Small **14**, 1801483 (2018).

[2] F. Miao, S.-J. Liang, and B. Cheng, Straintronics with van der Waals materials, npj Quantum Mater. **6**, 59 (2021).

[3] Z. Hennighausen and S. Kar, Twistronics: A turning point in 2D quantum materials, Electron. Struct. **3**, 014004 (2021).

[4] F. Xue, J.-H. He, and X. Zhang, Emerging van der Waals ferroelectrics: Unique properties and novel devices, Appl. Phys. Rev. **8**, 021316 (2021).

[5] Y. Zhou, D. Wu, Y. Zhu, Y. Cho, Q. He, X. Yang, K. Herrera, Z. Chu, Y. Han, M. C. Downer, H. Peng, and K. Lai, Out-of-Plane piezoelectricity and ferroelectricity in layered α-In_2Se_3 nanoflakes, Nano Lett. **17**, 5508 (2017).

[6] J. Xiao, H. Zhu, Y. Wang, W. Feng, Y. Hu, A. Dasgupta, Y. Han, Y. Wang, D. A. Muller, L. W. Martin, P. A. Hu, and X. Zhang, Intrinsic Two-Dimensional Ferroelectricity with Dipole Locking, Phys. Rev. Lett. **120**, 227601 (2018).

[7] F. Xue, W. Hu, K.-C. Lee, L.-S. Lu, J. Zhang, H.-L. Tang, A. Han, W.-T. Hsu, S. Tu, W.-H. Chang, C.-H. Lien, J.-H. He, Z. Zhang, L.-J. Li, and X. Zhang, Room-temperature ferroelectricity in hexagonally layered α-In_2Se_3 nanoflakes down to the monolayer limit, Adv. Funct. Mater. **28**, 1803738 (2018).

[8] M. Küpers, P. M. Konze, A. Meledin, J. Mayer, U. Englert, M. Wuttig, and R. Dronskowski, Controlled crystal growth of indium selenide, In_2Se_3, and the crystal structures of α-In_2Se_3, Inorg. Chem. **57**, 11775 (2018).

[9] R. Rashid, F. C.-C. Ling, S.-P. Wang, K. Xiao, X. Cui, Q. Rao, and D.-K. Ki, IP and OOP ferroelectricity in hexagonal γ-In_2Se_3 nanoflakes grown by chemical vapor deposition, J. Alloys Compd. **870**, 159344 (2021).

[10] M. Si, A. K. Saha, S. Gao, G. Qiu, J. Qin, Y. Duan, J. Jian, C. Niu, H. Wang, W. Wu, S. K. Gupta, and P. D. Ye, A ferroelectric semiconductor field-effect transistor, Nat. Electron. **2**, 580 (2019).

[11] K. Xu, W. Jiang, X. Gao, Z. Zhao, T. Low, and W. Zhu, Optical control of ferroelectric switching and multifunctional devices based on van der Waals ferroelectric semiconductors, Nanoscale **12**, 23488 (2020).

[12] Y. Su, X. Li, M. Zhu, J. Zhang, L. You, and E. Y. Tsymbal, Van der Waals multiferroic tunnel junctions, Nano Lett. **21**, 175 (2021).

[13] W. Qiao, D. Jin, W. Mi, D. Wang, S. Yan, X. Xu, and T. Zhou, Large perpendicular magnetic anisotropy of transition metal dimers driven by polarization switching of two-dimensional ferroelectric In_2Se_3 substrate, arXiv:2202.13726v1 (2022).

[14] K. Dou, W. Du, Y. Dai, B. Huang, and Y. Ma, 2D magnetoelectric multiferroics in MnSTe/In_2Se_3 heterobilayer with ferroelectrically controllable skyrmions, Phys. Rev. B **105**, 205427 (2022).

[15] M. Yudasaka, T. Matsuoka, and K. Nakanishi, Indium selenide film formation by the double-source evaporation of indium and selenium, Thin Solid Films **146**, 65 (1987).

[16] G. Gordillo and C. Calderón, CIS thin film solar cells with evaporated InSe buffer layers, Sol. Energy Mater. Sol. Cells **77**, 163 (2003).

[17] I.-H. Choi, The preparation of a $CuInSe_2$ solar cell by metal organic chemical vapor deposition, Thin Solid Films **525**, 137 (2012).

[18] C.-H. Ho and Y.-C. Chen, Thickness-tunable band gap modulation in γ-In_2Se_3, RSC Adv. **3**, 24896 (2013).

[19] A. Likforman, D. Carré, and R. Hillel, Structure cristalline du séléniure d'indium In_2Se_3, Acta Crystallogr., Sect. B **34**, 1 (1978).

[20] S. Marsillac, J. Bernede, R. L. Ny, and A. Conan, A new simple technique to obtain In_2Se_3 polycrystalline thin films, Vacuum **46**, 1315 (1995).

[21] A. Pfitzner and H. Lutz, Redetermination of the crystal structure of γ-In_2Se_3 by twin crystal x-ray method, J. Solid State Chem. **124**, 305 (1996).

[22] A. R. Barron, MOCVD of Group III chalcogenide compound semiconductors, MRS Proc. **335**, 317 (1993).

[23] P. O'Brien, D. J. Otway, and J. R. Walsh, The growth of indium selenide thin films from a novel asymmetric dialkyldiselenocarbamate of indium, Chem. Vap. Deposition **3**, 227 (1997).

[24] K. J. Chang, S. M. Lahn, and J. Y. Chang, Growth of single-phase In_2Se_3 by using metal organic chemical vapor deposition with dual-source precursors, Appl. Phys. Lett. **89**, 182118 (2006).

[25] M. D. Yang, C. H. Hu, S. C. Tong, J. L. Shen, S. M. Lan, C. H. Wu, and T. Y. Lin, Structural and optical characteristics of γ-In_2Se_3 nanorods grown on si substrates, J. Nanomater. **2011**, 976262 (2011).

[26] L. Brahim-Otsmane, J.-Y. Emery, and M. Eddrief, X-ray, reflection high electron energy diffraction and x-ray photoelectron spectroscopy studies of InSe and γ-In_2Se_3 thin films grown by molecular beam deposition, Thin Solid Films **237**, 291 (1994).

[27] C. Amory, J. C. Bernède, and S. Marsillac, Study of a growth instability of γ-In_2Se_3, J. Appl. Phys. **94**, 6945 (2003).

[28] T. Okamoto, A. Yamada, and M. Konagai, Growth and characterization of In_2Se_3 epitaxial films by molecular beam epitaxy, J. Cryst. Growth **175-176**, 1045 (1997).

[29] M. S. Claro, J. Grzonka, N. Nicoara, P. J. Ferreira, and S. Sadewasser, Wafer-scale fabrication of 2D β-In_2Se_3 photodetectors, Adv. Opt. Mater. **9**, 2001034 (2021).

[30] H. Lutz, M. Fischer, H.-P. Baldus, and R. Blachnik, Zur polymorphe des In_2Se_3, J. Less-Common Met. **143**, 83 (1988).

[31] X. Yin, X. Shen, C. Xu, J. He, J. Li, H. Ji, J. Wang, H. Li, X. Zhu, X. Niu, and Z. Wang, Monolithic epitaxy and optoelectronic properties of single-crystalline γ-In_2Se_3 thin films on mica, Chin. Phys. B **30**, 017701 (2021).

[32] J. Thomas, N. E. Weston, and T. E. O'Connor, Turbostratic boron nitride, thermal transformation to ordered-layer-lattice boron nitride, J. Am. Chem. Soc. **84**, 4619 (1962).

[33] M. Moret, A. Rousseau, P. Valvin, S. Sharma, L. Souqui, H. Pedersen, H. Högberg, G. Cassabois, J. Li, J. H. Edgar, and B. Gil, Rhombohedral and turbostatic boron nitride: X-ray diffraction and photoluminescence signatures, Appl. Phys. Lett. **119**, 262102 (2021).

[34] K. Kambas and C. Julien, Preparation and some optical and electrical measurements of a new phase α'-In_2Se_3, Mater. Res. Bull. **17**, 1573 (1982).

[35] S. Marsillac, A. Combot-Marie, J. Bernède, and A. Conan, Experimental evidence of the low-temperature formation of γ-In_2Se_3 thin films obtained by a solid-state reaction, Thin Solid Films **288**, 14 (1996).

[36] P. Giannozzi, O. Baseggio, P. Bonfà, D. Brunato, R. Car, I. Carnimeo, C. Cavazzoni, S. de Gironcoli, P. Delugas, F. Ferrari Ruffino, A. Ferretti, N. Marzari, I. Timrov, A. Urru, and S. Baroni, Quantum espresso toward the exascale, J. Chem. Phys. **152**, 154105 (2020).

[37] See Supplemental Material at http://link.aps.org/supplemental/10.1103/PhysRevMaterials.6.064003 for the crystal structure, the electronic band dispersion, the list of the Raman active modes, the zero-point gap renormalization, and additional optical data of the γ-In_2Se_3 films.

[38] M. Ueta, H. Kanzaki, K. K., Y. Toyozawa, and E. Hanamura, *Excitonic Processes in Solids*, edited by M. Cardona, P. Fulde, K. von Klitzing, and H.-J. Queisser, Vol. 60 (Springer-Verlag Berlin Heidelberg, 1986).

[39] M. Piacentini, E. Doni, R. Girlanda, V. Grasso, and A. Balzarotti, Electronic properties of the III-VI layer compounds GaS, GaSe and InSe, Il Nuovo Cimento B (1971-1996) **54**, 269 (1979).

[40] T. V. Shubina, W. Desrat, M. Moret, A. Tiberj, O. Briot, V. Y. Davydov, A. V. Platonov, M. A. Semina, and B. Gil, InSe as a case between 3D and 2D layered crystals for excitons, Nat. Commun. **10**, 3479 (2019).

[41] C. Klingshirn, *Semiconductor Optics* (Springer-Verlag Berlin Heidelberg, 2005).

[42] J. Dillinger, Č. Koňák, V. Prosser, J. Sak, and M. Zvára, Phonon-assisted exciton transitions in $A^{II} B^{VI}$ semiconductors, Phys. Status Solidi (b) **29**, 707 (1968).

[43] R. Le Toullec, N. Piccioli, and J. C. Chervin, Optical properties of the band-edge exciton in GaSe crystals at 10 K, Phys. Rev. B **22**, 6162 (1980).

[44] B. Gil, *Physics of Wurtzite Nitrides and Oxides: Passport to Devices* (Springer Series in Materials Science, Volume 197, Springer International Publishing, 2014).

[45] B. Gil, *Group III Nitride Semiconductor Compounds: Physics and Applications* (Clarendon Press Oxford, 1998).

[46] C. Julien, A. Chevy, and D. Siapkas, Optical properties of $In_2 Se_3$ phases, Phys. Status Solidi (a) **118**, 553 (1990).

[47] M. Cardona and M. L. W. Thewalt, Isotope effects on the optical spectra of semiconductors, Rev. Mod. Phys. **77**, 1173 (2005).

[48] Y. Varshni, Temperature dependence of the energy gap in semiconductors, Physica **34**, 149 (1967).

[49] L. Viña, S. Logothetidis, and M. Cardona, Temperature dependence of the dielectric function of germanium, Phys. Rev. B **30**, 1979 (1984).

[50] R. Pässler, Parameter Sets Due to Fittings of the Temperature Dependencies of Fundamental Bandgaps in Semiconductors, Phys. Status Solidi (b) **216**, 975 (1999).

[51] T. Q. P. Vuong, S. Liu, A. Van der Lee, R. Cuscó, L. Artús, T. Michel, P. Valvin, J. H. Edgar, G. Cassabois, and B. Gil, Isotope engineering of van der Waals interactions in hexagonal boron nitride, Nat. Mater. **17**, 152 (2018).

[52] T. Ohtsuka, T. Okamoto, A. Yamada, and M. Konagai, Photoluminescence study of γ-In_2 Se_3 epitaxial films grown by molecular beam epitaxy, J. Lumin. **87-89**, 293 (2000).

[53] Y.-C. Huang, Z.-Y. Li, W.-Y. Uen, S.-M. Lan, K. Chang, Z.-J. Xie, J. Chang, S.-C. Wang, and J.-L. Shen, Growth of γ-In_2 Se_3 films on Si substrates by metal-organic chemical vapor deposition with different temperatures, J. Cryst. Growth **310**, 1679 (2008).

[54] D. Lyu, T. Lin, T. Chang, S. Lan, T. Yang, C. Chiang, C. Chen, and H. Chiang, Structural and optical characterization of single-phase γ-In_2 Se_3 films with room-temperature photoluminescence, J. Alloys Compd. **499**, 104 (2010).

[55] N. Balakrishnan, E. D. Steer, E. F. Smith, Z. R. Kudrynskyi, Z. D. Kovalyuk, L. Eaves, A. Patanè, and P. H. Beton, Epitaxial growth of γ-InSe and α, β, and γ-In_2 Se_3 on ϵ-GaSe, 2D Mater. **5**, 035026 (2018).

[56] G. Davies, The optical properties of luminescence centres in silicon, Phys. Rep. **176**, 83 (1989).

[57] N. Kuroda, I. Munakata, and Y. Nishina, Exciton transitions from spin-orbit split off valence bands in layer compound InSe, Solid State Commun. **33**, 687 (1980).

[58] A. Segura, J. Bouvier, M. V. Andrés, F. J. Manjón, and V. Muñoz, Strong optical nonlinearities in gallium and indium selenides related to inter-valence-band transitions induced by light pulses, Phys. Rev. B **56**, 4075 (1997).

[59] G. F. Koster, J. O. Dimmock, R. G. Wheeler, and H. Statz, *Properties of the Thirty-Two Point Groups* (MIT Press, Cambridge, MA, 1963).

[60] M. Rose, *Elementary Theory of Angular Momentum* (Dover, New York, 1995).

[61] F. Bassani and G. Pastori Parravicini, *Electron States and Optical Transitions in Solids* (Pergamon Press, Oxford, New York, 1975).

[62] A. Baldereschi and M. Díaz, Anisotropy of excitons in semiconductors, Il Nuovo Cimento B **68**, 217 (1970).

[63] H. A. Bethe and R. W. Jackiw, *Intermediate Quantum Mechanics* (W. A. Benjamin Inc., New York, Amsterdam, 1968).

[64] J. F. Nye, *Physical Properties of Crystals: Their Representation by Tensors and Matrices* (Oxford University Press, Oxford, 1957).